

High field terahertz emission from relativistic laser-driven plasma wakefields

Zi-Yu Chen^{1,2, a)} and Alexander Pukhov¹

¹⁾*Institut für Theoretische Physik I, Heinrich-Heine-Universität Düsseldorf, Düsseldorf 40225, Germany*

²⁾*LSD, Institute of Fluid Physics, China Academy of Engineering Physics, Mianyang 621999, China*

(Dated: 16 October 2018)

We propose a method to generate high field terahertz (THz) radiation with peak strength of GV/cm level in the THz frequency gap range 1-10 THz using a relativistic laser interaction with a gaseous plasma target. Due to the effect of local pump depletion, an initially Gaussian laser pulse undergoes leading edge erosion and eventually evolves to a state with leading edge being step function. Interacting with such a pulse, electrons gain transverse residual momentum and excite net transverse currents modulated by the relativistic plasma frequency. These currents give rise to the low frequency THz emission. We demonstrate this process with one and two dimensional particle-in-cell simulations.

I. INTRODUCTION

High field terahertz (THz) pulses with peak electric field strength > 1 MV/cm in the previously hardly accessible THz frequency gap range 1-10 THz have gained wide scientific interest, since they offer attractive opportunities for studies in condensed matter physics, biology, chemistry and photonics. As a unique and versatile tool, high field THz sources not only allow probe and observe the state of matter with high sensitivity, but also open a door to manipulate and control the electronic, ionic and spin degrees of freedom of matter both resonantly and nonresonantly.¹

Currently, high field THz pulses can be generated from large-scale accelerators using ultrashort electron bunches. For example, peak field of 44 MV/cm has been obtained via coherent transition radiation in the Linac Coherent Light Source (LCLS).² In the laser-based schemes, THz pulses with field strength > 8 MV/cm at 1 KHz repetition rate have been generated via two-color laser filamentation.³ Single-cycle THz pulse with field strength up to 36 MV/cm can be generated by optical rectification of a midinfrared laser in a large-size nonlinear organic crystals assembly.⁴ In addition, other methods that have produced high field THz pulses include difference frequency mixing process of two near-infrared lasers in second-order nonlinear crystals, but only with components > 20 THz,⁵ and optical rectification in lithium niobate (LiNbO₃) crystals with tilted laser front, but mostly limited to < 1.5 THz.⁶ Besides, high field THz source can be generated from relativistic laser irradiated plasmas via various mechanisms.⁷⁻¹⁰

In our previous work, we have shown numerically that THz pulses with field strength > 1 GV/cm can be generated in plasma wakefields by use of temporally tailored laser pulses.¹¹ The mechanism is related to the excitation of transverse plasma current via electron residual momentum left by the temporally tailored laser pulse.

For an electron initially at rest, the transverse momentum p_z normalized by $m_e c$ after the interaction with a z -polarized laser pulse can be obtained as an integral of the transverse field E_z :¹²

$$p_z = a_z = e/(m_e c) \int_{-\infty}^{+\infty} E_z(\eta) d\eta, \quad (1)$$

where a_z is the normalized vector potential, $\eta = t - x/c$, e is the elementary charge, m_e is the electron mass, and c is the speed of light in vacuum. After the interaction with a normal Gaussian pulse, the above integral is zero, and hence electrons gain no net energy. However, if the laser pulse has such a steepened edge that it becomes a step function, a large transverse residual momentum p_z^R as well as vector potential a_z^R will be generated. Considering the one-dimensional (1D) wave equation¹³

$$\left(\partial_x^2 - \frac{1}{c^2} \partial_t^2\right) a_z^T = \left(\frac{\omega_{p0}}{c}\right)^2 s_z(x, t) \quad (2)$$

with the source term

$$s_z(x, t) = \frac{n_e(x, t) a_z^R(x, t)}{\gamma(x, t)}, \quad (3)$$

where a_z^T is the vector potential of the THz wave, $\omega_{p0} = (4\pi n_0 e^2 / m_e)^{1/2}$ is the background plasma frequency, $n_e(x, t)$ is the plasma density normalized by the initial density n_0 , and γ is the relativistic Lorentz factor. The normalized THz electric field by $m_e \omega_0 c / e$ can then be obtained as

$$e_z^T(x, t) = -\frac{1}{\omega_0} \partial_t a_z^T = \frac{\omega_{p0}}{2\omega_0} \int_{-\infty}^{+\infty} \frac{dx'}{l_s} s_z(x', t - |x - x'|/c), \quad (4)$$

where $l_s = c/\omega_{p0}$ and ω_0 is the laser angular frequency.

In this work, we demonstrate that THz emission from laser plasma wakefields can be self-consistently realized with a normal Gaussian laser pulse, unlike previously the laser pulse with a step-function edge is introduced artificially.¹¹ The way to achieve the required pulse shape is to utilize the effect of localized etching. When a high

^{a)} Electronic mail: Ziyu.Chen@uni-duesseldorf.de

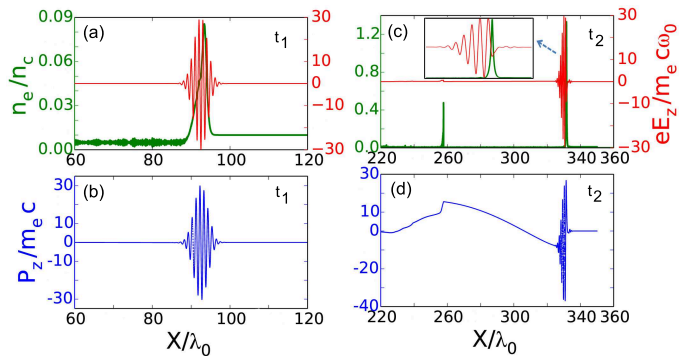


FIG. 1. (Color online) Spatial profiles of the electron density n_e (green) and transverse field E_z (red) at (a) $t_1 = 80T_0$ and (c) $t_2 = 318T_0$. (b) and (d) are the corresponding spatial distribution of the transverse momentum P_z for (a) and (c), respectively. The inset of (c) shows a close-up for the laser pulse shape.

intensity laser pulse propagates in underdense plasmas, the leading edge of the laser pulse can get eroded and depleted via the local pump depletion mechanism,¹⁴ and thus eventually evolves to a state with a step-function front. The net transverse current exited by such a pulse in the plasma wakefields, modulated by the relativistic plasma frequency, should be capable of generating low frequency THz pulses.

II. SIMULATION RESULTS AND DISCUSSIONS

To illustrate the THz generation process, 1D particle-in-cell (PIC) simulations have been carried out using the Virtual Laser Plasma Laboratory (VLPL) code.¹⁵ A circularly polarized laser with a Gaussian temporal profile $a(t) = a_0 \exp(-t^2/\tau_0^2)$ is normally incident along the x -axis, where a_0 and τ_0 are respectively the laser normalized peak amplitude and the pulse duration. We note that linearly polarized laser also works. Here, we take $a_0 = eE_0/m_e c \omega_0 = 30$ with E_0 the laser electric field amplitude. The pulse duration is about 11 fs full-width at half-maximum (FWHM). The laser wavelength is taken to be $\lambda_0 = 0.8 \mu\text{m}$. A fully ionized plasma is initially located between $50\lambda_0$ and $350\lambda_0$. For the laser intensities and plasma densities we considered here, the usual gas jets routinely used in experiments can be employed, such as hydrogen, helium and nitrogen gases.^{16,17} For simplicity, a homogeneous plasma slab with a density of $n_0 = 0.01n_c$ is used, where $n_c = m_e \omega_0^2 / 4\pi e^2 \sim 10^{21} \text{ W/cm}^2$ is the critical plasma density. We also checked inhomogeneous density profiles with density gradients and find this mechanism also works. The simulation box length is $550\lambda_0$. The grid size is $\lambda_0/100$ with each cell filled with 10 macroparticles.

Figure 1 shows the snapshots of distribution of the laser pulse E_z and the electron density n_e as well as the transverse momentum of electron P_z at two different

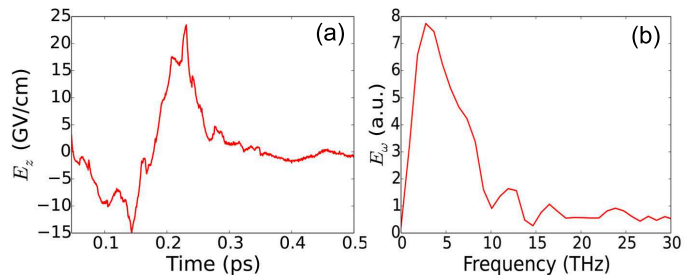


FIG. 2. (Color online) (a) Temporal waveform and (b) the corresponding Fourier spectrum of the forward THz emission field E_z observed in front of the right plasma-vacuum boundary.

times: $t_1 = 80T_0$ and $t_2 = 318T_0$, where T_0 is the laser period. In Fig. 1(a), an electron density peak is formed at the front of the laser pulse by snow plowing the electrons forward due to the laser ponderomotive force. The peak electron density is larger than the initial background density, but still much smaller than the critical density. The laser pulse almost holds its initial symmetric temporal shape. The corresponding transverse momentum P_z in Fig. 1(b) only exists inside the laser pulse. Behind the laser pulse, one finds $P_z \approx 0$. From Fig. 1(c), however, one can see that at a later time, the density peak at the front of the pulse becomes narrow and sharp. The amplitude of the density spike is above the critical density. This results in an efficient erosion of the leading edge of the pulse due to localized energy depletion mechanism within the narrow density spike region.¹⁴ As the laser pulse propagates, the density spike is continuously pushed by the laser ponderomotive force in front of the pulse. Consequently, the laser front coincides with the density spike where it depletes its pump energy. Due to the etching of the front, the laser pulse evolves to a state with an ultra-steep front which is approximately a step function (see a close-up for the laser pulse shape in the inset of Fig. 1(c)). As the laser front continuously etches backwards, the sharp shape of the leading edge is kept. Although there are some other effects like group velocity steepening that can lead to the formation of steep pulse front,¹⁸ these processes are not so efficient. With this pulse shape of step-function front, the integral in Eq. (1) is no longer zero. As a result, the electrons acquire a net transverse momentum after the interaction with the laser field. This residual momentum left behind the laser pulse can be clearly seen in Fig. 1(d). Due to the residual momentum, the plasma electrons keep on a free oscillation with the background plasma frequency ω_p . Then a low frequency transverse net current is built up in the plasma wakefields and emits both forward and backward low frequency electromagnetic radiation through the plasma slab.¹⁹ We note that the second density peak at around $260 \lambda_0$ behind the laser pulse in Fig. 1(c) is a trapped electron sheet injected into the wakefield. This electron sheet may generate an ultrafast XUV pulse in the presence of the residual transverse momentum.²⁰

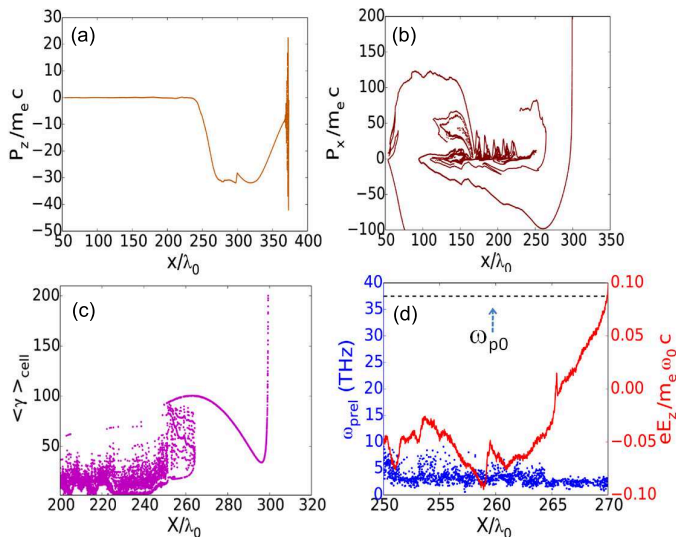


FIG. 3. (Color online) (a) $x - p_z$ and (b) $x - p_x$ phase space distributions of the electrons. (c) Spatial distribution of the relativistic γ -factor. (d) Spatial profiles of the relativistic plasma frequency ω_{prel} (blue) and the transverse electric field E_z (red) in the skin layer. The black dashed line marks the initial plasma frequency ω_{p0} . The time is $t = 360T_0$.

The temporal waveform and the corresponding Fourier spectrum of the low frequency emission observed in the forward direction are shown in Figs. 2(a) and (b), respectively. A single-cycle THz pulse is obtained, which lasts for a few hundred femtoseconds. The peak field strength of the THz pulse reaches about 24 GV/cm. The spectral shape shows that most of the pulse energy concentrates in the desired THz frequency gap range of 1-10 THz, with a peak frequency of about 3 THz.

The initial plasma frequency is $\omega_{p0} \approx 37.5$ THz, which is greater than the central frequency of the observed THz emission. This can be attributed to the change of the plasma frequency due to relativistic effects. As a result of the interaction with the relativistic laser, electrons reach near light speed and gain a large Lorentz factor ($\gamma = 1/\sqrt{1 - (v/c)^2}$). Therefore, the mass of electron is increased and the effective plasma frequency is reduced. The relativistically corrected expression for the plasma frequency is $\omega_{\text{prel}} = (4\pi e^2 n_e(x)/\gamma m_e)^{1/2}$. We plot the electrons' γ -factor along with the phase space distribution at time $t = 360T_0$ in Figs. 3 (a)-(c). The γ -factor is obtained by averaging the values in each cell, i.e., $\gamma = \langle \gamma \rangle_{\text{cell}}$. In the skin layer near the plasma rear surface, large residual transverse momentum can be seen, which can excite net transverse currents radiating electromagnetic pulses (see Fig. 3(a)). In this plasma region, the Lorentz factor γ of the bulk electrons reaches up to 100 (see Fig. 3(c)). In addition to the bulk electrons, there are some high-energy electrons with $\gamma > 100$, which can also be seen in Fig. 3(b). These electrons are refluxing backwards in the electrostatic field due to charge separation with the ions. Unlike the bulk electrons, they

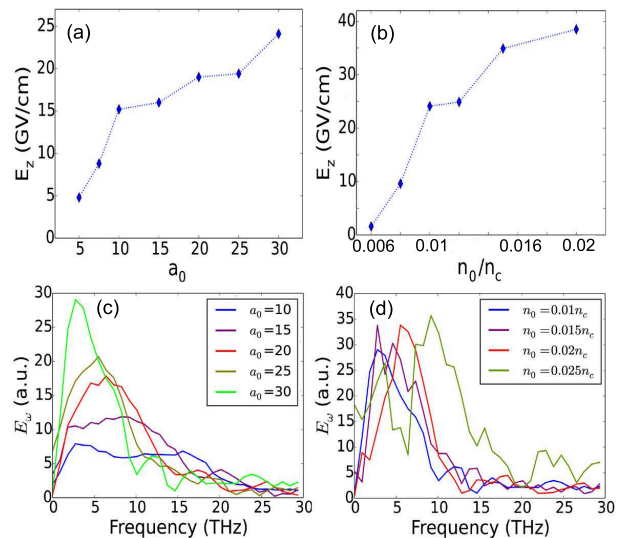


FIG. 4. (Color online) (a)-(b): Peak THz field strength as a function of (a) the driven laser amplitude a_0 and (b) the initial plasma density n_0 . (c)-(d): THz spectrum dependence on (c) a_0 and (d) n_0 . The plasma density is $n_0 = 0.01n_c$ for panels (a) and (c). The laser amplitude is $a_0 = 30$ for panels (b) and (d).

contribute little to the plasma frequency. Figure 3(d) shows the profiles of the relativistic plasma frequency $\omega_{\text{prel}}(x, t)$ and the transverse electric field $E_z(x, t)$ in the skin layer. The initial undisturbed plasma frequency ω_{p0} is marked as the black dashed line. Due to the relativistic effect, the effective plasma frequency is largely decreased to be around a few THz, which is in the THz frequency gap range. The net transverse current modulated by this plasma frequency leads to the emission at the low THz frequencies.

We find the present scheme works for a wide range of laser and plasma parameters. Figure 4 presents the results of a series of simulations, where we take $n_0 = 0.01n_c$ in panels (a) and (c), and $a_0 = 30$ in panels (b) and (d). Figs. 4 (a) and (b) shows the peak amplitude of the THz emission increases with increase of the driver strength a_0 and the plasma density n_0 . Higher a_0 and n_0 both lead to a higher density spike in front of the laser pulse, which results in a more efficient local depletion of the laser energy, and thus a stronger radiation field. A rough scaling of the THz strength dependence on the laser plasma parameters can be obtained using the above 1D model. Assuming the source is sharply localized and exponentially decays in the skin depth l_s , the integral of Eq. (4) can be approximated by $e_z^T \simeq \omega_p s_z / 2\omega_0$.^{13,19} Concerning the source term, we further assume that the driver laser is nonevolving. With the assumption of the quasistatic approximation,²¹ the plasma fluid quantities can then be expressed as $n_e/n_0 = [\gamma_{\perp}^2 + (1 + \phi^2)]/2(1 + \phi)^2$ and $\gamma = [\gamma_{\perp}^2 + (1 + \phi^2)]/2(1 + \phi)$, where $\gamma_{\perp}^2 = 1 + a^2$ and ϕ is the electrostatic wake potential.²² In the near wavebreaking nonlinear limit $(1 + \phi) \rightarrow 1/\gamma_p$, where the

plasma Lorentz factor $\gamma_p = (1 - v_p^2/c^2)^{-1/2}$ with v_p the phase velocity of the plasma wave. Then the THz field can be obtained as $e_z^T \propto \omega_{p0} a_z^R \gamma_p$.

The THz spectrum dependence on the laser intensity and plasma density are shown in Figs. 4(c) and (d), respectively. With increasing the laser intensity, both the spectrum width and the central frequency decrease, and the peak spectral strength increases. The red shift of the central frequency is due to a lower relativistic plasma frequency, as a consequence of a larger γ -factor. Since the emitted pulse is single cycle, a lower-frequency (longer-wavelength) pulse has a longer temporal duration, and thus a narrower bandwidth. From Fig. 4(d) one can see that the central THz frequency increases with increasing the plasma density, which is due to an increased plasma frequency. These results may offer a way to obtain a tunable THz source.

In the following we present 2D PIC simulation results to check the present scheme working in multi-dimensional geometries. The size of the simulation box is $550\lambda_0 \times 60\lambda_0$ in the xy plane and the grid step is $\lambda_0/50 \times \lambda_0/20$. The laser amplitude is $a_0 = 30$ and the spot size is $15 \mu\text{m}$ FWHM. The plasma density is $n_0 = 0.02n_c$. Figures 5(a) and (c) show the 2D snapshots of distribution of the transverse electric field E_z and the electron density n_e at time $t = 300T_0$, respectively. The corresponding line-out plots along $Y = 0$ are shown in Fig. 5(b) and (d). As in the 1D case, the laser pulse drives an electron density spike at the front. The leading edge is eroding and becoming ultra-steep. Figures 5(e) and (f) show a snapshot of the electric field E_z , i.e., the distribution of the forward emission, and its corresponding Fourier spectrum along $Y = 0$ at time $t = 500T_0$. The inset of Fig. 5(f) shows the line-out plot of the THz electric field along $Y = 0$. One can see that the emission fields also have strong peaks in the THz frequency gap range of < 10 THz. The peak field strength is about 0.3 GV/cm. The reduction of the field strength can be attributed to multi-dimensional effects such as transverse electron spreading and wave diffraction. In the 1D cases, the dense electron spike in front of the laser pulse maintains for a long time, provided the laser ponderomotive force is much larger than the electrostatic restoring force. In the multi-dimensional cases, the transverse spreading effects reduce both the average density and lifetime of the electron spike, which consequently impair the efficiency of the laser front etching and THz generation. Further increasing the plasma density and focusing the THz emission may result in a higher field strength.

III. CONCLUSIONS

In conclusion, we have proposed a method to generate high field THz radiation using a relativistic laser interaction with gaseous plasma targets. An initially Gaussian laser pulse snow plows electrons forward to form a sharp density spike in front of the pulse. Due to the

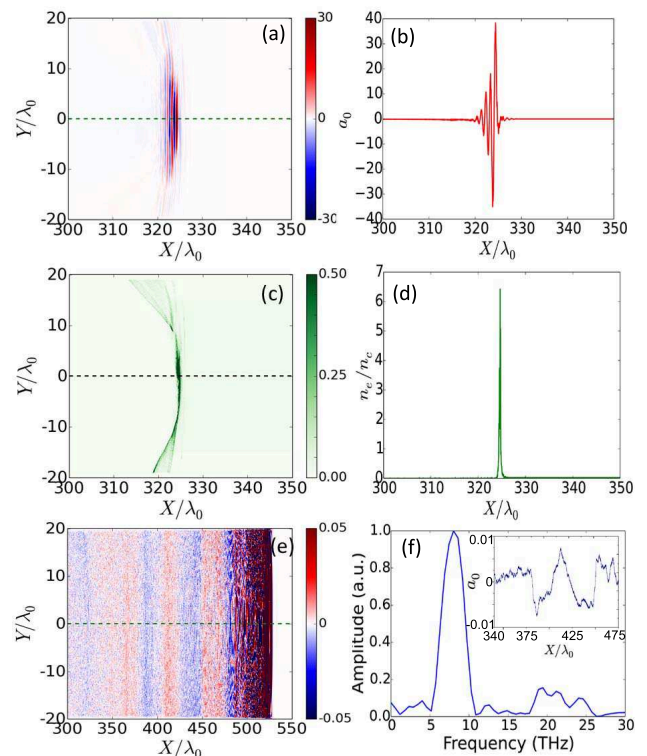


FIG. 5. (Color online) Results from 2D simulations. (a) A snapshot of the transverse electric field $eE_z/m_e\omega_0c$ distribution and (b) the corresponding line-out plot along $Y = 0$ at time $t = 300T_0$. (c) A snapshot of the density n_e distribution and (d) its line-out profile along $Y = 0$ at $t = 300T_0$. (e) A snapshot of the forward emission field $eE_z/m_e\omega_0c$ distribution and (f) the Fourier spectrum of the field along $Y = 0$ at $t = 500T_0$. The inset of panel (f) shows the line-out plot of the THz field along $Y = 0$, which was smoothed to get rid of the numerical noise.

local pump depletion effect, the laser front is gradually etched to become a step-function state. Plasma electrons gain a net residual momentum after interaction with such a pulse and excite transverse oscillations modulated by the relativistic plasma frequency, which emits the low frequency THz pulses. This result opens the way for experimental approaches. This tunable THz source with a peak field strength reaching GV/cm level and spectrum mainly within the THz gap range, should be of interest for high-field THz science and applications.

ACKNOWLEDGMENTS

Z.-Y. C. acknowledges financial support from the China Scholarship Council (CSC). This work was supported by the Deutsche Forschungsgemeinschaft SFB TR 18 and by EU FP7 project EUCARD-2.

¹T. Kampfrath, K. Tanaka, and K. A. Nelson, Nat. Photonics **7**, 680 (2013)

- ²Z. Wu, A. S. Fisher, J. Goodfellow, M. Fuchs, H. Wen, S. Ghimire, D. A. Reis, H. Loos, and A. Lindenberg, *Rev. Sci. Instrum.* **84**, 022701 (2013)
- ³T. I. Oh, Y. J. Yoo, Y. S. You, and K. Y. Kim, *Appl. Phys. Lett.* **105**, 041103 (2014)
- ⁴C. Vicario, B. Monozslai, and C. P. Hauri, *Phys. Rev. Lett.* **112**, 213901 (2014)
- ⁵A. Sell, A. Leitenstorfer, and R. Huber, *Opt. Lett.* **33**, 2767 (2008)
- ⁶A. G. Stepanov, S. Henin, Y. Petit, L. Bonacina, J. Kasparian, and J.-P. Wolf, *Appl. Phys. B* **115**, 293 (2014)
- ⁷Z.-M. Sheng, K. Mima, J. Zhang, and H. Sanuki, *Phys. Rev. Lett.* **94**, 095003 (2005)
- ⁸Y. T. Li, C. Li, M. L. Zhou, W. M. Wang, F. Du, W. J. Ding, X. X. Lin, F. Liu, Z. M. Sheng, X. Y. Peng, L. M. Chen, J. L. Ma, X. Lu, Z. H. Wang, Z. Y. Wei, and J. Zhang, *Appl. Phys. Lett.* **100**, 254101 (2012)
- ⁹A. Gopal, S. Herzer, A. Schmidt, P. Singh, A. Reinhard, W. Ziegler, D. Brommel, A. Karmakar, P. Gibbon, U. Dillner, T. May, H.-G. Meyer, and G. G. Paulus, *Phys. Rev. Lett.* **111**, 074802 (2013)
- ¹⁰Z.-Y. Chen, X.-Y. Li, and W. Yu, *Phys. Plasmas* **20**, 103115 (2013)
- ¹¹Z.-Y. Chen, *Appl. Phys. Lett.* **102**, 241104 (2013)
- ¹²B. J. Galow, Y. I. Salamin, T. V. Liseykina, Z. Harman, and C. H. Keitel, *Phys. Rev. Lett.* **107**, 185002 (2011)
- ¹³R. Lichters, J. Meyer-ter-Vehn, and A. Pukhov, *Phys. Plasmas* **3**, 3425 (1996)
- ¹⁴C. D. Decker, W. B. Mori, K.-C. Tzeng, and T. Katsouleas, *Phys. Plasmas* **3**, 2047 (1996)
- ¹⁵A. Pukhov, *J. Plasma Phys.* **61**, 425 (1999)
- ¹⁶K. Huang, D. Z. Li, W. C. Yan, M. H. Li, M. Z. Tao, Z. Y. Chen, X. L. Ge, F. Liu, Y. Ma, J. R. Zhao, N. M. Hafz, J. Zhang, and L. M. Chen, *Appl. Phys. Lett.* **105**, 204101 (2014)
- ¹⁷W. C. Yan, L. M. Chen, D. Z. Li, L. Zhang, N. A. M. Hafz, J. Dunn, Y. Ma, K. Huang, L. N. Su, M. Chen, Z. M. Sheng, and J. Zhang, *Proc. Natl. Acad. Sci. USA* **111**, 5825 (2014)
- ¹⁸J. Vieira, F. Fiuza, L. O. Silva, M. Tzoufras, and W. B. Mori, *New J. Phys.* **12**, 045025 (2010)
- ¹⁹H.-C. Wu, Z.-M. Sheng, and J. Zhang, *Phys. Rev. E* **77**, 046405 (2008)
- ²⁰Y. Liu, Z. M. Sheng, J. Zheng, F. Y. Li, X. L. Xu, W. Lu, W. B. Mori, C. S. Liu, and J. Zhang, *New J. Phys.* **14**, 083031 (2012)
- ²¹P. Sprangle, E. Esarey, and A. Ting, *Phys. Rev. A* **41**, 4463 (1990)
- ²²E. Esarey, C. B. Schroeder, and W. P. Leemans, *Rev. Mod. Phys.* **81**, 1229 (2009)